



The $K^- \pi^+$ S-wave from the $D^+ \rightarrow K^- \pi^+ \pi^+$ decay [☆]

FOCUS Collaboration

J.M. Link^a, P.M. Yager^a, J.C. Anjos^b, I. Bediaga^b, C. Castromonte^b, A.A. Machado^b, J. Magnin^b, A. Massafferri^b, J.M. de Miranda^b, I.M. Pepe^b, E. Polycarpo^b, A.C. dos Reis^{b,*}, S. Carrillo^c, E. Cuautle^c, A. Sánchez-Hernández^c, C. Uribe^c, F. Vázquez^c, L. Agostino^d, L. Cinquini^d, J.P. Cumalat^d, V. Frisullo^d, B. O'Reilly^d, I. Segoni^d, K. Stenson^d, J.N. Butler^e, H.W.K. Cheung^e, G. Chiodini^e, I. Gaines^e, P.H. Garbincius^e, L.A. Garren^e, E. Gottschalk^e, P.H. Kasper^e, A.E. Kreymer^e, R. Kutschke^e, M. Wang^e, L. Benussi^f, S. Bianco^f, F.L. Fabbri^f, A. Zallo^f, E. Casimiro^g, M. Reyes^g, C. Cawfield^h, D.Y. Kim^h, A. Rahimi^h, J. Wiss^h, R. Gardnerⁱ, A. Kryemadhiⁱ, Y.S. Chung^j, J.S. Kang^j, B.R. Ko^j, J.W. Kwak^j, K.B. Lee^j, K. Cho^k, H. Park^k, G. Alimonti^l, S. Barberis^l, M. Boschini^l, A. Cerutti^l, P. D'Angelo^l, M. DiCorato^l, P. Dini^l, L. Edera^l, S. Erba^l, P. Inzani^l, F. Leveraro^l, S. Malvezzi^l, D. Menasce^l, M. Mezzadri^l, L. Moroni^l, D. Pedrini^l, C. Pontoglio^l, F. Prelz^l, M. Rovere^l, S. Sala^l, T.F. Davenport III^m, V. Arenaⁿ, G. Bocaⁿ, G. Bonomiⁿ, G. Gianiniⁿ, G. Liguoriⁿ, D. Lopes Pegnaⁿ, M.M. Merloⁿ, D. Panteaⁿ, S.P. Rattiⁿ, C. Riccardiⁿ, P. Vituloⁿ, C. Göbel^o, J. Otalora^o, H. Hernandez^p, A.M. Lopez^p, H. Mendez^p, A. Paris^p, J. Quinones^p, J.E. Ramirez^p, Y. Zhang^p, J.R. Wilson^q, T. Handler^r, R. Mitchell^r, D. Engh^s, M. Hosack^s, W.E. Johns^s, E. Luiggi^s, J.E. Moore^s, M. Nehring^s, P.D. Sheldon^s, E.W. Vaandering^s, M. Webster^s, M. Sheaff^t

^a University of California, Davis, CA 95616, United States

^b Centro Brasileiro de Pesquisas Físicas, Rio de Janeiro, RJ, Brazil

^c CINVESTAV, 07000 México City, DF, Mexico

^d University of Colorado, Boulder, CO 80309, United States

^e Fermi National Accelerator Laboratory, Batavia, IL 60510, United States

^f Laboratori Nazionali di Frascati dell'INFN, Frascati I-00044, Italy

^g University of Guanajuato, 37150 Leon, Guanajuato, Mexico

^h University of Illinois, Urbana-Champaign, IL 61801, United States

ⁱ Indiana University, Bloomington, IN 47405, United States

^j Korea University, Seoul, Republic of Korea 136-701

^k Kyungpook National University, Taegu 702-701, Republic of Korea

^l INFN and University of Milano, Milano, Italy

^m University of North Carolina, Asheville, NC 28804, United States

ⁿ Dipartimento di Fisica Nucleare e Teorica and INFN, Pavia, Italy

^o Pontifícia Universidade Católica, Rio de Janeiro, RJ, Brazil

^p University of Puerto Rico, Mayaguez, PR 00681, United States

^q University of South Carolina, Columbia, SC 29208, United States

^r University of Tennessee, Knoxville, TN 37996, United States

^s Vanderbilt University, Nashville, TN 37235, United States

^t University of Wisconsin, Madison, WI 53706, United States

ARTICLE INFO

Article history:

Received 4 June 2009

Received in revised form 24 July 2009

Accepted 24 September 2009

Available online 29 September 2009

Editor: M. Doser

PACS:

10.

13.25.Es

0370-2693 © 2009 Elsevier B.V. Open access under CC BY license.

doi:10.1016/j.physletb.2009.09.057

ABSTRACT

Using data from FOCUS (E831) experiment at Fermilab, we present a model independent partial-wave analysis of the $K^- \pi^+$ S-wave amplitude from the decay $D^+ \rightarrow K^- \pi^+ \pi^+$. The S-wave is a generic complex function to be determined directly from the data fit. The P- and D-waves are parameterized by a sum of Breit–Wigner amplitudes. The measurement of the S-wave amplitude covers the whole elastic range of the $K^- \pi^+$ system.

© 2009 Elsevier B.V. Open access under CC BY license.

13.25.Ft
 13.75.Lb
 14.40.Aq
 14.40.Lb

1. Introduction

Over forty years have passed since the birth of the Constituent Quark Model, yet the scalar mesons still challenge theoreticians and experimentalists. Many states have been reported. Some still need confirmation, others need to have better measurements of the pole position and couplings to specific channels. The identification of the nature of each state – regular $q\bar{q}$ mesons, tetraquarks, molecules, glueballs – is a major task which will only be accomplished combining results from different types of data.

An important problem is the understanding of the low energy part of the S-wave $K^-\pi^+$ spectrum, where the existence of an $I = 1/2$ state, the $\kappa(800)$ meson, has been the subject of a long-standing debate. Evidence for a neutral low mass scalar state in heavy flavor decays has been reported by several experiments [1–4]. The pole position has been determined recently using Roy–Steiner representations of $K^-\pi^+$ scattering [5]. However, evidence for the charged partner is still scarce and conflicting [6,7].

The primary source for the $K\pi \rightarrow K\pi$ scattering has been the data from the classic LASS experiment [8], $K^-p \rightarrow K^-\pi^+n$. With a cut at low momentum transfers, the K^-p interaction is assumed to be entirely due to the one-pion-exchange mechanism. The incident pion is, therefore, not a real, asymptotically free particle, but a nearly on-shell virtual state. An additional cut on the π^+n mass was set to avoid baryonic intermediate states. The LASS analysis was performed on a sample containing 151 thousand events. With this sample LASS found that the $K\pi$ cross section is elastic up to the $K\eta'$ threshold ($1.454 \text{ GeV}/c^2$). Unfortunately, LASS data start only at $m_{K\pi} = 825 \text{ MeV}/c^2$.

Heavy flavor decays are currently the only way to access the whole elastic range of the $K\pi$ spectrum, starting from threshold. A golden mode for the neutral $K\pi$ system is the decay $D^+ \rightarrow K^-\pi^+\pi^+$ (charge conjugate states are always implied), which has a largely dominant S-wave component – a common feature of three-body final states with identical pions.

Dalitz plot analyses are performed in the framework of the so-called Isobar Model [9]. While the modeling of the P- and D-waves are common to most analyses, several forms of representing the S-wave have been used, namely the coherent sum of a uniform nonresonant amplitude plus Breit–Wigner functions for the scalar resonances – hereafter called the Isobar Model for the S-wave, the K-matrix formalism and the Model-Independent Partial Wave Analysis (MIPWA). The BaBar Collaboration [6] uses the $I = 1/2$ elastic scattering amplitude from LASS for the $K\pi$ S-wave. Another approach is the non-parametric analysis of the $K\pi$ amplitude from the $D^+ \rightarrow K^-K^+\pi^+$ decay performed by FOCUS [10].

The $D^+ \rightarrow K^-\pi^+\pi^+$ decay was already studied by the Fermilab FOCUS Collaboration [3]. In our previous work the $D^+ \rightarrow K^-\pi^+\pi^+$ Dalitz plot was analyzed with the K-matrix formalism for the $K^-\pi^+$ S-wave. As a cross check, a fit with the usual Isobar Model for the S-wave was also performed. The K-matrix formalism was applied for the first time in Dalitz plot analysis of D decays in the FOCUS study of the $D^+ \rightarrow \pi^+\pi^-\pi^+$ decay [11].

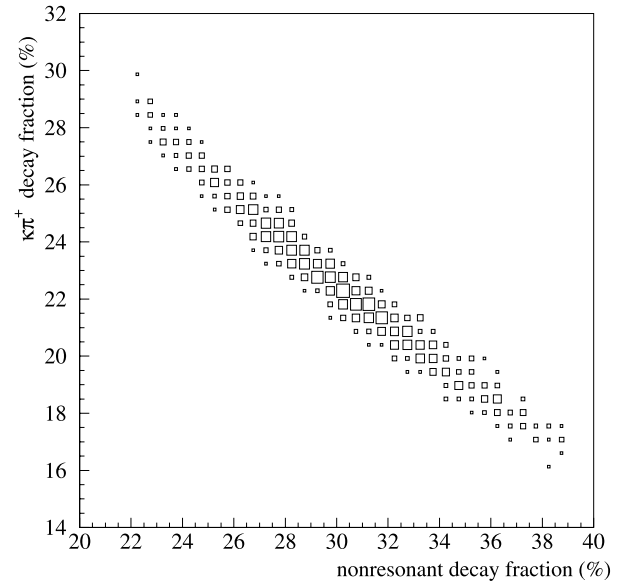


Fig. 1. Correlation between nonresonant and $\kappa\pi^+$ decay fractions in the isobar model. An ensemble of $D^+ \rightarrow K^-\pi^+\pi^+$ Dalitz plots was simulated and fitted with the isobar model. The scatter plot shows a high correlation between the two largest contributions of the S-wave.

In the Isobar Model the S-wave is represented by a coherent sum of a uniform nonresonant term plus two relativistic Breit–Wigner amplitudes. A good fit can be achieved, but it is difficult to determine the relative amount of each S-wave component. In order to illustrate the correlation between the S-wave components of the isobar model an ensemble of 2,000 $D^+ \rightarrow K^-\pi^+\pi^+$ Dalitz plots was simulated using the set of parameters from our isobar fit (Table 2 of Ref. [3]). Each simulated Dalitz plot was fitted and a scatter plot of the nonresonant versus $\kappa(800)\pi^+$ decay fractions is presented in Fig. 1. One can clearly see that a better description of the S-wave requires one to go beyond the isobar model.

The K-matrix formalism is based on the assumption that there is no three-body final state interaction. In this approach the dynamics of the $K^-\pi^+\pi^+$ final state are driven by the $K^-\pi^+$ system. Data on D decays and on scattering would be directly related and the two-body unitarity would become a constraint. The evolution of the $K^-\pi^+$ pair is fixed to that of $K\pi$ elastic scattering, considering the contribution of both $I = 1/2$ and $I = 3/2$ $K^-\pi^+$ amplitudes. The parameters of the $K^-\pi^+$ production amplitude and the relative amount and phase of the two isospin components are determined by the fit. A good description of the data was obtained, with an important contribution of the $I = 3/2$ $K\pi$ amplitude. The production amplitude has a slowly varying phase. The conclusion of this study is that data on D decays and scattering are consistent. The three-body final state interactions would, therefore, play a marginal role.

In this Letter we complete our study of the $D^+ \rightarrow K^-\pi^+\pi^+$ Dalitz plot, applying the MIPWA technique, developed by the E791 Collaboration [12], to the same data set used for the K-matrix and Isobar fits [3]. In the MIPWA method, the $K^-\pi^+$ S-wave amplitude is parameterized by a generic complex function, to be determined directly from the data. The only assumption common to all other Dalitz plot analyses is that the P- and D-waves are well repre-

☆ See <http://www-focus.fnal.gov/authors.html> for additional author information.

* Corresponding author.

E-mail address: alberto@cbpf.br (A.C. dos Reis).

sented by a sum of Breit–Wigner amplitudes. The $K^-\pi^+$ mass spectrum is divided into slices. The magnitude and phase of the S-wave component at the edge of each slice are determined by the fit. A cubic spline interpolation is used to obtain the S-wave magnitude and phase at any point in the spectrum.

The MIPWA technique provides a model-independent way to determine the $K^-\pi^+$ S-wave amplitude. The result, however, is inclusive. The measured phase, in addition to the $l = 1/2$ $K^-\pi^+$ phase, may contain contributions from the $l = 3/2$ components, as well as possible contributions from three-body final state interactions.

The Letter is organized as follows. In the next section we describe the selection of the data sample. The MIPWA formalism is described in Section 3. The results of the MIPWA fit are presented in Section 4.

2. The $D^+ \rightarrow K^-\pi^+\pi^+$ sample

FOCUS is a charm photo-production experiment which collected data during the 1996–1997 fixed target run at Fermilab. The photon beam was produced by means of bremsstrahlung, from electron and positron beams (typically with 300 GeV endpoint energy). The electron/positron beams were obtained from the 800 GeV Tevatron proton beam. The photon beam interacted with a segmented BeO target [13]. The mean photon energy for reconstructed charm events is ~ 180 GeV.

The FOCUS spectrometer has a system of three multi-cell threshold Čerenkov counters to perform the charged particle identification, separating kaons from pions up to a momentum of 60 GeV/c. The identification and separation of charm primary (production) and secondary (decay) vertices are made by two systems of silicon micro-vertex detectors. The first system consists of 4 planes of micro-strips interleaved with the experimental target [14] and the second system consists of 12 planes of micro-strips located downstream of the target. The charged particle momentum is determined by measuring the deflections in two magnets of opposite polarity through five stations of multi-wire proportional chambers.

The data set used in this analysis is the same as in Ref. [3]. The final states are selected using a *candidate driven vertex algorithm* [15]. A secondary vertex is formed from the three candidate tracks. The momentum of the resultant D^+ candidate is used as a *seed* track to intersect the other reconstructed tracks and to search for a primary vertex. The primary vertex must have at least two reconstructed tracks in addition to the D^+ seed. The confidence level of each vertex is required to be greater than 1%. Once the production and decay vertices are determined, the distance L between the vertices and its error σ_L are computed. The quantity L/σ_L is an unbiased measure of the significance of detachment between the primary and secondary vertices. This is the most important criterion for separating charm events from non-charm prompt backgrounds. Signal quality is further enhanced by isolation requirements. Tracks forming the D candidate vertex must have a confidence level smaller than 0.001% to form a vertex with the tracks from the primary vertex. In addition, all remaining tracks not assigned to either the primary or the secondary vertex must have a confidence level smaller than 0.1% to form a vertex with the D candidate daughters.

Particle identification criteria used in FOCUS are based on likelihood ratios between the various particle identification hypotheses. These likelihoods are computed for a given track from the observed firing response (on or off) of all the cells that are within the track's ($\beta = 1$) Čerenkov cone for each of our three Čerenkov counters. The product of all firing probabilities for all the cells within the three Čerenkov cones produces a χ^2 -like variable $W_i =$

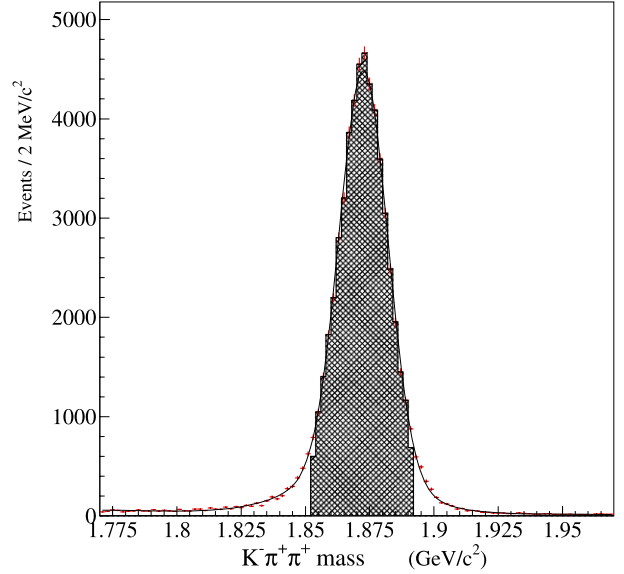


Fig. 2. The $K^-\pi^+\pi^+$ invariant mass distribution.

$-2\ln(\text{Likelihood})$ where i ranges over the electron, pion, kaon and proton hypotheses [16]. The kaon track is required to have $\Delta_K = W_\pi - W_K$ greater than 3; both pion candidates are required to satisfy $\Delta_\pi = W_K - W_\pi$ greater than 3; in addition, all tracks are required to be separated by less than 5 units from the best hypothesis, that is $\Delta W = W_{\min} - W_K < 5$ and $\Delta W = W_{\min} - W_\pi < 5$. These Čerenkov requirements reduce the contamination of $D_s^+ \rightarrow K^-K^+\pi^+$ background to a negligible level.

Using the selection criteria just described, we obtain the invariant $K^-\pi^+\pi^+$ mass distribution shown in Fig. 2. The mass plot of Fig. 2 is fitted with a function that includes two Gaussian functions with different widths and the same mean, which take into account differences in the resolution in the momentum determination of our spectrometer [15], and an exponential function for the background. The events used in the MIPWA fit correspond to the shaded area in Fig. 2, i.e., events with $1.8515 < M_{K\pi\pi} < 1.9031$ GeV/c². Events in this mass region that lie outside the kinematic limit defined by the nominal D^+ mass are discarded. The final data subset contains 53,595 events, with a purity ($S/(S+B)$) of 98.8%.

The symmetrized Dalitz plot of these events (two entries per event) is shown in Fig. 3. A narrow band corresponding to the $D^+ \rightarrow \bar{K}^*(892)^0\pi^+$ events can be clearly seen. The asymmetry in each $\bar{K}^*(892)^0$ lobe is evident and it is caused by the interference between this state and the $K^-\pi^+$ S-wave. Indeed, it is this interference with the P-wave that allows one to access the S-wave phase.

3. The model independent partial-wave analysis formalism

In the MIPWA formalism the Dalitz plot of Fig. 3 is described by a coherent sum of three partial waves, corresponding to the $K^-\pi^+$ system in the angular momentum states $L = 0, 1$ and 2. The partial waves are complex functions of the two $K\pi$ invariant masses squared, $s_a = (p_K + p_{\pi_a})^2$ and $s_b = (p_K + p_{\pi_b})^2$, which specify the kinematics of the $D^+ \rightarrow K^-\pi_a^+\pi_b^+$ decay. Each partial wave is Bose-symmetrized with respect to the identical pions,

$$\mathcal{A}_L = A_L(s_a, s_b) + A_L(s_b, s_a). \quad (1)$$

The $K^-\pi^+$ S-wave amplitude is an unknown complex function of the $K^-\pi^+$ mass squared,

$$A_0(s_a, s_b) = a_0(s_a)e^{i\phi_0(s_a)} + a_0(s_b)e^{i\phi_0(s_b)}. \quad (2)$$

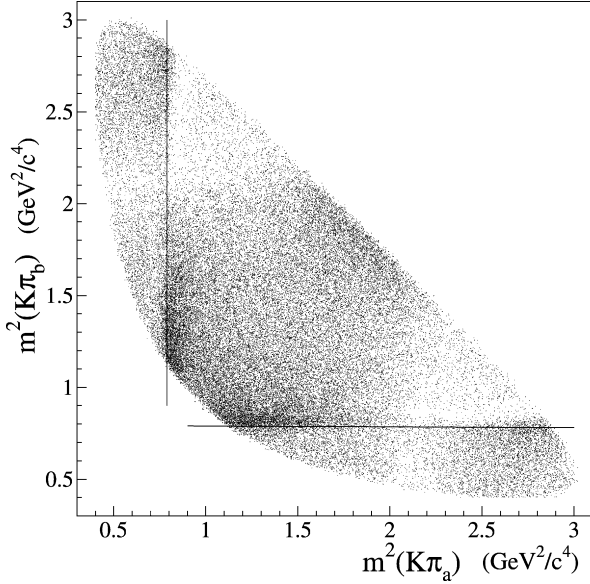


Fig. 3. The $K^-\pi^+\pi^+$ Dalitz plot.

No assumption about the content of the S-wave is made: the real functions $a_0(s)$ and $\phi_0(s)$ are determined directly by the Dalitz plot fit. The $K^-\pi^+$ mass spectrum is divided into 39 slices of the same size. For each of the 40 endpoints s_k there are two free parameters, a_k and ϕ_k , defining the function $A_0(s_a, s_b)$ at that position. A cubic spline interpolation is used to define the values of both $a_0(s)$ and $\phi_0(s)$ between $s_k \leq s < s_{k+1}$. The S-wave has, therefore, a set of 40 pairs (a_k, ϕ_k) of fit parameters.

The $K^-\pi^+$ P-wave amplitude has two components, namely the $\bar{K}^*(892)^0\pi^+$, taken as the reference mode, and the $\bar{K}^*(1680)^0\pi^+$,

$$A_1(s_a, s_b) = F_1^D(s_a, s_b) F_1^R(s_a, s_b) [c_0 BW_{K^*(892)}(s_a) + c_1 BW_{K^*(1680)}(s_a)] \mathcal{M}_1(s_a, s_b). \quad (3)$$

The D-wave has only one component, the $\bar{K}_2^*(1430)\pi^+$ mode,

$$A_2(s_a, s_b) = c_2 [F_2^D(s_a, s_b) F_2^R(s_a, s_b) BW_{K_2^*(1430)}(s_a)] \mathcal{M}_2(s_a, s_b). \quad (4)$$

The complex coefficients c_i are also fit parameters, except for c_0 , the coefficient of the reference mode, which is fixed to 1.0.

In the above equations F^D and F^R are the usual Blatt-Weisskopf form factors [17],

$$F_{L=1} = [1 + (rq)^2]^{-1/2}, \quad (5)$$

and

$$F_{L=2} = [9 + 3(rq)^2 + (rq)^4]^{-1/2}, \quad (6)$$

where q is the momentum of the resonance decay products in the resonance rest frame. The form factor parameters $r = r_D$ for the D decay vertex, and $r = r_R$ for the resonance decay, are fixed at the values used in Ref. [3]: $r_D = 1.5 \text{ (GeV}/c)^{-1}$ and $r_R = 5.0 \text{ (GeV}/c)^{-1}$.

The functions \mathcal{M}_L are the spin amplitudes, accounting for angular momentum conservation. For a spin-1 resonance $D^+ \rightarrow R\pi_b^+$, $R \rightarrow K^-\pi_a^+$ the corresponding spin amplitude is

$$\mathcal{M}_{L=1} = \sum_M p_{\pi_b}^\mu e_\mu(p, M) e_\nu(p, M) (p_{\pi_a} - p_K)^\nu, \quad (7)$$

where e_μ is the resonance polarization vector with magnetic quantum number M , p is the momentum 4-vector and p_i^μ are the

momenta of the final state particles. After summing over the unobserved resonance polarization states, the spin amplitude reduces to

$$\mathcal{M}_{L=1} = -2 |\vec{p}_{\pi_b}| |\vec{p}_K| \cos \theta, \quad (8)$$

where θ is the cosine of the angle formed by \vec{p}_K and \vec{p}_{π_b} in the resonance rest frame.

In the case of the $\bar{K}_2^*(1430)\pi^+$ mode, the spin amplitude is

$$\mathcal{M}_{L=2} = \sum_M p_{\pi_b}^\mu p_{\pi_b}^\nu e_\mu(p, M) e_\nu(p, M) e_\alpha(p, M) e_\beta(p, M) \times (p_{\pi_a} - p_K)^\alpha (p_{\pi_a} - p_K)^\beta, \quad (9)$$

which, after summing over the resonance polarization, reduces to

$$\mathcal{M}_{L=2} = \frac{4}{3} (|\vec{p}_{\pi_b}| |\vec{p}_K|)^2 (3 \cos^2 \theta - 1). \quad (10)$$

The relativistic Breit-Wigner has an energy dependent width,

$$BW = \frac{1}{s - s_0 + i\sqrt{s_0} \Gamma_{\text{tot}}(s)}, \quad (11)$$

where s is the $K^-\pi^+$ mass squared, s_0 the resonance nominal mass and

$$\Gamma_{\text{tot}}(s) = \Gamma_0 \sqrt{\frac{s_0}{s}} \left(\frac{q}{q_0}\right)^{2L+1} \frac{F_L^2(q)}{F_L^2(q_0)}, \quad (12)$$

where L is the orbital angular momentum in the rest frame of the decaying resonance.

The signal distribution is corrected on an event-by-event basis for the acceptance. The acceptance is determined by a full Monte Carlo simulation of events: the $\gamma - N$ interaction, event propagation through the spectrometer, event reconstruction and event retention according to the selection criteria described in Section 2. The resulting distribution of Monte Carlo events varies smoothly over the Dalitz plot and the acceptance function is obtained by fitting this distribution to a 10th order polynomial.

The signal distribution is corrected on an event-by-event basis for the acceptance. The acceptance is determined by a full Monte Carlo simulation of events: the $\gamma - N$ interaction, event propagation through the spectrometer, event reconstruction and event retention according to the selection criteria described in Section 2. The observed distribution of Monte Carlo events varies smoothly over the Dalitz plot and the acceptance function is obtained by fitting this distribution to a 10th order polynomial.

The signal probability distribution is normalized to unity,

$$P_S(s_a, s_b) = \frac{1}{N_S} \varepsilon(s_a, s_b) \left| \sum \mathcal{A}_L \right|^2, \quad (13)$$

where $\varepsilon(s_a, s_b)$ is the acceptance function and N_S the overall normalization constant,

$$N_S = \int ds_a ds_b \varepsilon(s_a, s_b) \left| \sum \mathcal{A}_L \right|^2. \quad (14)$$

The background probability distribution is fixed in the fit. The background shape is determined by a fit to the Dalitz plot of events from the $K^+\pi^-\pi^-$ mass sidebands [3]. The signal fraction is estimated by a fit to the $K^+\pi^-\pi^-$ mass spectrum.

In the MIPWA fit there are $40 \times 2 + 2 \times 2 = 84$ free parameters. The optimum set of parameters is determined by an unbinned maximum likelihood fit, minimizing the quantity $w \equiv -2 \ln(L)$, where the likelihood function, L , is given by

$$L = \prod_{\text{events}} [f_S P_S^i(s_a, s_b) + (1 - f_S) P_B^i(s_a, s_b)], \quad (15)$$

where f_S is the signal fraction $f_S = S/(S+B)$.

Table 1
Decay fractions (%) and phases, in degrees, from the three FOCUS $K\pi\pi$ Dalitz plot fits.

Mode	FOCUS MIPWA	FOCUS K-matrix	FOCUS isobar model
$K^-\pi^+$ S-wave	$80.24 \pm 1.38 \pm 0.23 \pm 0.25 \pm 0.26$	$83.23 \pm 1.50 \pm 0.04 \pm 0.07$	–
$\bar{K}^*(892)^0\pi^+$	$12.36 \pm 0.34 \pm 0.19 \pm 0.16 \pm 0.23$ 0 (fixed)	$13.61 \pm 0.41 \pm 0.01 \pm 0.30$ 0 (fixed)	$13.7 \pm 0.4 \pm 0.6 \pm 0.3$ 0 (fixed)
$\bar{K}^*(1410)^0\pi^+$	– –	$0.48 \pm 0.21 \pm 0.012 \pm 0.17$ ($293 \pm 17 \pm 0.4 \pm 7$)°	$0.2 \pm 0.1 \pm 0.1 \pm 0.04$ ($350 \pm 34 \pm 17 \pm 15$)°
$\bar{K}^*(1680)^0\pi^+$	$1.75 \pm 0.62 \pm 0.24 \pm 0.23 \pm 0.42$ ($67 \pm 6 \pm 2 \pm 2 \pm 3$)°	$1.90 \pm 0.65 \pm 0.01 \pm 0.43$ ($1 \pm 7 \pm 0.2 \pm 6$)°	$1.8 \pm 0.4 \pm 0.2 \pm 0.3$ ($3 \pm 7 \pm 4 \pm 8$)°
$\bar{K}_2^*(1430)\pi^+$	$0.58 \pm 0.1 \pm 0.04 \pm 0.03 \pm 0.04$ ($336 \pm 7 \pm 3 \pm 2 \pm 2$)°	$0.39 \pm 0.1 \pm 0.004 \pm 0.05$ ($296 \pm 7 \pm 0.3 \pm 1$)°	$0.4 \pm 0.05 \pm 0.04 \pm 0.03$ ($319 \pm 8 \pm 2 \pm 2$)°
$\bar{K}_0^*(1430)\pi^+$	– –	– –	$17.5 \pm 1.5 \pm 0.8 \pm 0.4$ ($36 \pm 5 \pm 2 \pm 1.2$)°
$\kappa\pi^+$	– –	– –	$22.4 \pm 3.7 \pm 1.2 \pm 1.5$ ($199 \pm 6 \pm 1 \pm 5$)°
nonresonant	– –	– –	$29.7 \pm 4.5 \pm 1.5 \pm 2.1$ ($325 \pm 4 \pm 2 \pm 1.2$)°
$\chi^2/\text{d.o.f.}$	1.08	1.27	1.17
C.L.	6.8%	1.2%	6.8%

In the MIPWA column the first error is statistical, the second and third errors are, respectively, our estimate of the *split sample* and *fit variant* systematic uncertainties, and the last error is the systematic error due to the uncertainty in the parameters of the other waves. Goodness of fit are also shown for the three models.

Decay fractions are obtained from the coefficients c_k , determined by the fit, and after integrating the overall signal amplitude over the phase space,

$$f_k = \frac{\int ds_a ds_b |c_k \mathcal{A}_k(s_a, s_b)|^2}{\int ds_a ds_b |\sum_j c_j \mathcal{A}_j(s_a, s_b)|^2}. \quad (16)$$

Errors on the fractions include errors on both magnitudes and phases, and are computed using the full covariance matrix.

4. Results of the MIPWA

The decay fractions resulting from the MIPWA fit are presented in Table 1. For comparison, the third and fourth columns have the fractions from our previous fits using the K-matrix formalism and the isobar model.¹

The data is well described by a P-wave model with two components. No improvement in the fit quality is observed when a third component, the $\bar{K}^*(1410)\pi^+$ mode, is added. The contribution of this mode is consistent with zero. As in previous analyses of the $D^+ \rightarrow K^+\pi^-\pi^-$ Dalitz plot, the S-wave component is dominant. The decay fractions from the MIPWA and from our previous K-matrix Dalitz plot fit are in good agreement.

In Table 2 the MIPWA decay fractions are compared to the ones from E791 and CLEO-c. Our results are in good agreement with the decay fractions from E791. The total S-wave contribution from CLEO-c is significantly higher if we add the binned S-wave and the $\bar{K}_0^*(1430)\pi^+$ fractions.

The fitted values of the S-wave magnitudes and phases are presented in Table 3 and plotted in Figs. 4 and 5. The error bars in these figures contain the statistical and systematic errors added in quadrature. The dashed line in Fig. 4 indicates the $K\eta'$ threshold, the upper limit of the region where the $K^-\pi^+$ amplitude is predominantly elastic [8].

¹ The two statistical errors here reported on the $\bar{K}^*(892)^0\pi^+$ decay fraction for both the K-matrix and isobar fits are smaller than those quoted in Ref. [3]. They were overestimated in Ref. [3] as a consequence of a minor mistake in the error propagation code, which affected their computation only and not those of the other fit fractions. The two new values reported here are the correct ones, and should replace the old ones.

Table 2
Decay fractions (%) and phases, in degrees, from the MIPWA Dalitz plot fit compared to E791 and CLEO-c.

Mode	FOCUS MIPWA	E791	CLEO-c
$K^-\pi^+$ S-wave	$80.24 \pm 1.38 \pm 0.23 \pm 0.25 \pm 0.26$	78.6 ± 2.3	83.8 ± 3.8
$\bar{K}_0^*(1430)\pi^+$	– –	– –	13.3 ± 0.62 51 (fixed)
$\bar{K}^*(892)^0\pi^+$	$12.36 \pm 0.34 \pm 0.19 \pm 0.16 \pm 0.23$ 0 (fixed)	11.9 ± 2.0 0 (fixed)	9.88 ± 0.46 0 (fixed)
$\bar{K}^*(1680)^0\pi^+$	$1.75 \pm 0.62 \pm 0.24 \pm 0.23 \pm 0.42$ ($67 \pm 6 \pm 2 \pm 2 \pm 3$)°	1.2 ± 1.2 (43 ± 17)°	0.20 ± 0.12 (113 ± 14)°
$\bar{K}_2^*(1430)\pi^+$	$0.58 \pm 0.1 \pm 0.04 \pm 0.03 \pm 0.04$ ($336 \pm 7 \pm 3 \pm 2 \pm 2$)°	0.2 ± 0.1 (-12 ± 29)°	0.20 ± 0.04 (15 ± 9)°

The S-wave phase grows continuously across the elastic region, starting at -138° and with a total variation of 200° . After a sudden drop near the $\bar{K}_0^*(1430)$ mass, the phase becomes nearly constant.

The S-wave magnitude is a decreasing function up to $m_{K\pi} \simeq 1.2 \text{ GeV}/c^2$. There is a dip near the $\bar{K}_0^*(1430)$ mass, which is most readily explained by the interference between the different components of the S-wave.

The measured magnitudes are more affected by the systematic uncertainties than are the measured phases. In both cases the systematic uncertainties are comparable to or larger than the statistical errors.

4.1. Goodness-of-fit

For all fits the goodness-of-fit is accessed through a two-dimensional χ^2 test, using an adaptive binning algorithm. The folded Dalitz plot is divided into 844 cells of variable size, with a minimum occupancy of 50 data events, in such a way that all cells have a nearly equal and sufficiently large population. This procedure allows us to test the fit quality in great detail across the Dalitz plot. For each cell we define the χ^2 as

$$\chi_i^2 = \frac{(n_{\text{obs}} - n_{\text{exp}})^2}{\sigma_{\text{exp}}^2}. \quad (17)$$

Table 3
Magnitudes and phases of the S-wave from MIPWA fit.

$K^-\pi^+$ mass (GeV/c ²)	a (GeV/c ²) ⁻²	ϕ (degrees)
0.63	2.31 ± 0.24 ± 0.02 ± 0.07 ± 0.19 (0.20)	-138 ± 10 ± 2 ± 4 ± 6 (7)
0.66	1.76 ± 0.14 ± 0.07 ± 0.06 ± 0.13 (0.16)	-121 ± 7 ± 2 ± 3 ± 6 (7)
0.69	2.07 ± 0.14 ± 0.08 ± 0.06 ± 0.13 (0.16)	-119 ± 6 ± 3 ± 3 ± 5 (7)
0.72	1.95 ± 0.15 ± 0.01 ± 0.08 ± 0.14 (0.16)	-108 ± 5 ± 2 ± 3 ± 6 (7)
0.75	1.68 ± 0.17 ± 0.05 ± 0.09 ± 0.13 (0.17)	-92 ± 6 ± 3 ± 2 ± 6 (7)
0.77	1.95 ± 0.16 ± 0.01 ± 0.07 ± 0.15 (0.16)	-97 ± 5 ± 3 ± 2 ± 5 (6)
0.80	1.61 ± 0.11 ± 0.05 ± 0.07 ± 0.15 (0.16)	-73 ± 5 ± 1 ± 2 ± 7 (7)
0.83	1.69 ± 0.12 ± 0.04 ± 0.09 ± 0.15 (0.17)	-70 ± 4 ± 4 ± 1 ± 4 (6)
0.86	1.56 ± 0.15 ± 0.06 ± 0.08 ± 0.14 (0.16)	-67 ± 3 ± 4 ± 0 ± 2 (7)
0.89	1.65 ± 0.17 ± 0.03 ± 0.05 ± 0.16 (0.17)	-61 ± 2 ± 2 ± 0 ± 2 (3)
0.91	1.75 ± 0.16 ± 0.05 ± 0.06 ± 0.18 (0.19)	-53 ± 3 ± 2 ± 0 ± 2 (3)
0.94	1.70 ± 0.11 ± 0.04 ± 0.03 ± 0.15 (0.17)	-49 ± 4 ± 2 ± 0 ± 2 (3)
0.97	1.58 ± 0.07 ± 0.04 ± 0.05 ± 0.13 (0.14)	-31 ± 7 ± 2 ± 1 ± 4 (5)
1.00	1.61 ± 0.06 ± 0.03 ± 0.05 ± 0.10 (0.12)	-31 ± 6 ± 3 ± 1 ± 4 (5)
1.03	1.58 ± 0.05 ± 0.03 ± 0.03 ± 0.10 (0.11)	-23 ± 6 ± 1 ± 1 ± 3 (3)
1.06	1.69 ± 0.05 ± 0.04 ± 0.03 ± 0.14 (0.15)	-26 ± 5 ± 2 ± 0 ± 2 (3)
1.08	1.60 ± 0.05 ± 0.02 ± 0.03 ± 0.12 (0.13)	-17 ± 4 ± 2 ± 0 ± 2 (3)
1.11	1.53 ± 0.05 ± 0.04 ± 0.02 ± 0.13 (0.13)	-11 ± 4 ± 1 ± 0 ± 2 (2)
1.14	1.52 ± 0.05 ± 0.03 ± 0.01 ± 0.11 (0.11)	-9 ± 3 ± 2 ± 0 ± 1 (2)
1.17	1.60 ± 0.05 ± 0.01 ± 0.01 ± 0.10 (0.10)	0 ± 3 ± 1 ± 0 ± 1 (1)
1.20	1.60 ± 0.05 ± 0.05 ± 0.01 ± 0.08 (0.09)	-1 ± 3 ± 1 ± 0 ± 1 (1)
1.22	1.67 ± 0.05 ± 0.05 ± 0.01 ± 0.07 (0.08)	-1 ± 3 ± 1 ± 1 ± 1 (2)
1.25	1.71 ± 0.05 ± 0.04 ± 0.01 ± 0.11 (0.12)	7 ± 4 ± 1 ± 1 ± 1 (2)
1.28	1.77 ± 0.05 ± 0.05 ± 0.01 ± 0.11 (0.12)	7 ± 4 ± 1 ± 1 ± 1 (2)
1.31	1.78 ± 0.05 ± 0.04 ± 0.02 ± 0.10 (0.11)	9 ± 4 ± 2 ± 1 ± 2 (3)
1.34	1.69 ± 0.05 ± 0.01 ± 0.02 ± 0.10 (0.10)	15 ± 4 ± 1 ± 1 ± 2 (3)
1.36	1.74 ± 0.06 ± 0.05 ± 0.02 ± 0.10 (0.11)	24 ± 4 ± 1 ± 1 ± 2 (3)
1.39	1.69 ± 0.06 ± 0.07 ± 0.01 ± 0.11 (0.13)	26 ± 5 ± 1 ± 1 ± 2 (3)
1.42	1.39 ± 0.07 ± 0.05 ± 0.01 ± 0.09 (0.11)	31 ± 6 ± 2 ± 2 ± 3 (6)
1.45	1.04 ± 0.08 ± 0.01 ± 0.03 ± 0.10 (0.10)	48 ± 6 ± 3 ± 3 ± 4 (6)
1.48	0.66 ± 0.09 ± 0.01 ± 0.05 ± 0.09 (0.11)	64 ± 7 ± 1 ± 3 ± 5 (6)
1.51	0.52 ± 0.06 ± 0.01 ± 0.01 ± 0.11 (0.11)	23 ± 12 ± 1 ± 4 ± 4 (6)
1.53	0.48 ± 0.05 ± 0.04 ± 0.06 ± 0.08 (0.11)	-6 ± 13 ± 1 ± 4 ± 6 (7)
1.56	0.80 ± 0.05 ± 0.06 ± 0.05 ± 0.09 (0.12)	-23 ± 9 ± 1 ± 2 ± 5 (6)
1.59	1.15 ± 0.07 ± 0.03 ± 0.08 ± 0.08 (0.11)	-29 ± 8 ± 1 ± 1 ± 4 (4)
1.62	1.43 ± 0.06 ± 0.04 ± 0.05 ± 0.09 (0.11)	-15 ± 7 ± 1 ± 2 ± 3 (4)
1.65	1.56 ± 0.08 ± 0.06 ± 0.09 ± 0.10 (0.14)	-19 ± 7 ± 3 ± 1 ± 3 (4)
1.67	1.71 ± 0.10 ± 0.02 ± 0.08 ± 0.11 (0.13)	-15 ± 8 ± 3 ± 2 ± 3 (5)
1.70	1.53 ± 0.13 ± 0.04 ± 0.10 ± 0.12 (0.16)	-24 ± 9 ± 4 ± 2 ± 4 (6)
1.73	1.60 ± 0.16 ± 0.06 ± 0.10 ± 0.15 (0.19)	-34 ± 14 ± 5 ± 3 ± 6 (8)

The first error is statistical. The second and third errors are, respectively, our estimate of the *split sample* and *fit variant* systematic uncertainties, whereas the last error is the systematic error due to the uncertainty in the parameters of the other waves. The full systematic error is a sum in quadrature of these three errors. This is the number between parentheses.

In the above expression n_{exp} is the expected population of each cell, given by a Monte Carlo simulation performed with 1,000,000 events generated according to the model resulting from the MIPWA fit, and σ_{exp} is the uncertainty on this number. The overall χ^2 is a sum of the χ_i^2 over all cells. The number of degrees-of-freedom is given by the number of cells minus the number of fit parameters. From these two quantities we estimate the confidence level of our fits.

The overall χ^2 of the MIPWA fit is $\chi^2 = 818.8$ ($844 - 84 = 760$ degrees of freedom), which corresponds to a confidence level of 6.8%. The χ^2 distribution across the Dalitz plot is shown in Fig. 6.

The Dalitz plot projections (highest and lowest $K^-\pi^+$ invariant mass squared) are plotted in Fig. 7, with the fit result superimposed (solid histograms).

4.2. Systematic uncertainties

Systematic uncertainties may come from different sources. We have performed *split sample* studies, in which the data was divided into four sets of independent samples, according to the parent

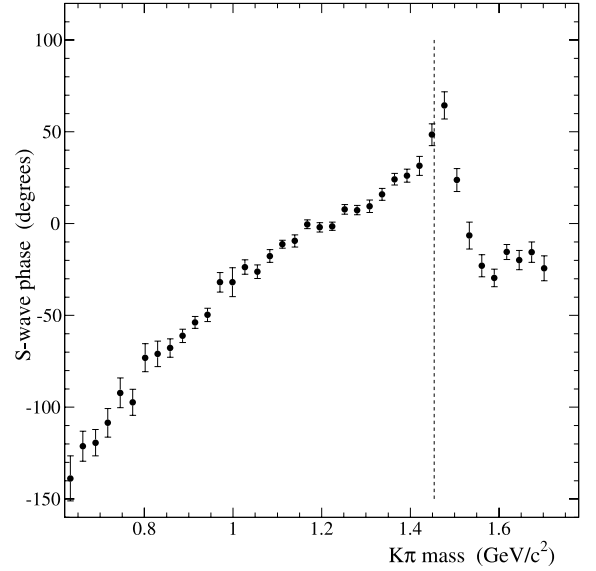


Fig. 4. The S-wave phase as a function of the $K^-\pi^+$ mass from the MIPWA $K^-\pi^+\pi^+$ Dalitz plot fit. The hashed vertical line shows the elastic range according to LASS.

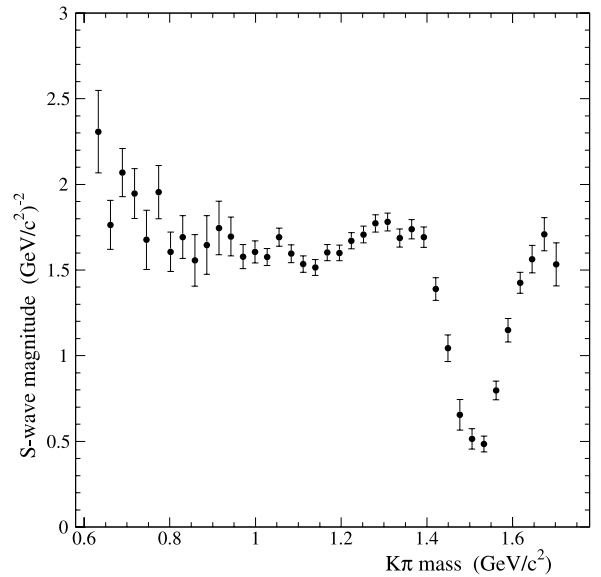


Fig. 5. The S-wave magnitude as a function of the $K^-\pi^+$ mass from the MIPWA $K^-\pi^+\pi^+$ Dalitz plot fit.

D meson charge and momentum. The *split sample* component takes into account the possible systematics introduced by a residual difference between data and Monte Carlo, due to a possible mismatch in the reproduction of the D^+ production. A technique, employed in FOCUS and modeled after the *S-factor method* from the Particle Data Group [9], was used to try to separate true systematic variations from statistical fluctuations. We found a small effect from the *split sample* studies.

A second class of studies is the *fit variant*, in which the fit of the whole data set is performed under different conditions. Fit variants included changes in the background level and in the first derivatives of the spline at the edges of the $K^-\pi^+$ spectrum. The *fit variant* component is estimated by the *r.m.s.* of the measurements.

The third and dominant source of systematic errors comes from the uncertainty in the parameters of the P- and D-waves. This includes uncertainties on the values of the parameters r_R and r_D . We

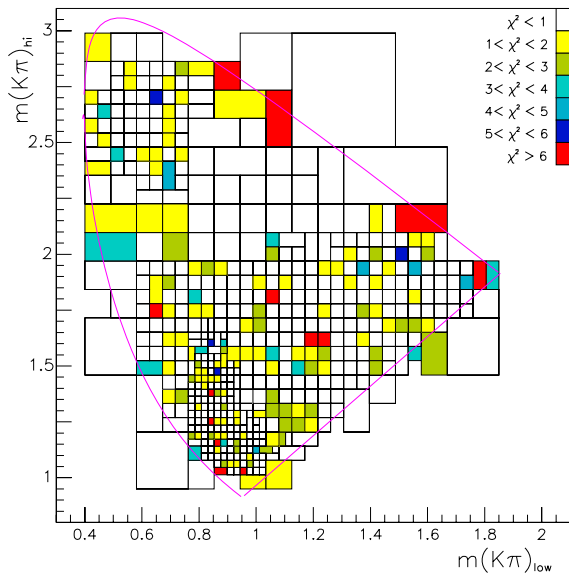


Fig. 6. The χ^2 distribution across the folded Dalitz plot.

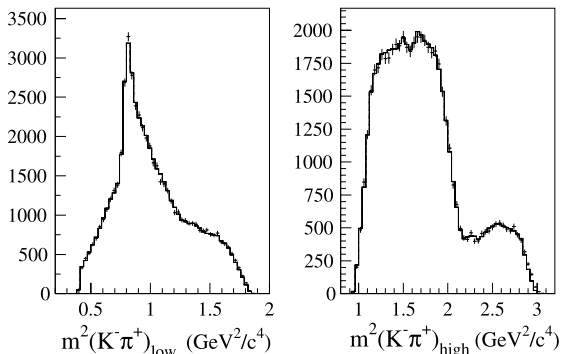


Fig. 7. Comparison between the $K^-\pi^+\pi^+$ Dalitz plot projections and the MIPWA fit, with the lowest (left plot) and highest (right plot) $K^-\pi^+$ invariant mass squared. In the plots the solid histogram is a projection of the fit.

repeated the fit changing by $\pm 1\sigma$, one at a time, the values of the mass and width of the high-mass vector resonances, according to the PDG, and of the parameters r_R and r_D . This component is also estimated by the *r.m.s.* of the measurements.

The contributions of each source are quoted individually in Tables 1, 2 and 3. The overall systematic uncertainty was obtained adding in quadrature the three components described above, and corresponds to the values in parentheses in Table 3.

5. Summary and conclusions

A Dalitz plot fit was performed with the MIPWA technique. The $K^-\pi^+$ S-wave amplitude was determined directly from data, with no assumption about its nature. The only hypotheses are that the decay amplitude can be described by a sum of partial waves, and that the P- and D-waves are well described by a coherent sum of Breit–Wigner amplitudes.

The MIPWA decay fractions are in good agreement with our previous analysis and with the E791 results. A large dominance of the S-wave component is observed in this decay.

The phase of the S-wave amplitude grows continuously across the elastic range, with a total variation of approximately 200° . At the $K^-\pi^+$ threshold there is a phase difference of approximately -140° between the S- and P-waves.

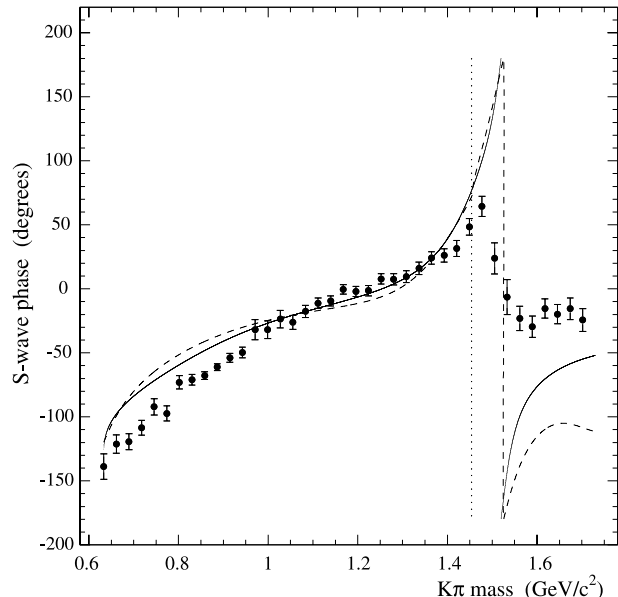


Fig. 8. Comparison between the S-wave phase from the three different FOCUS fits of the $K^-\pi^+\pi^+$ Dalitz plot. Points with error bars are the result of the MIPWA fit. The solid line is the central value of the isobar fit. The dashed line is the result of the K-matrix fit.

The phase variation of the S-wave measured in this analysis and that of E791 agree well, specially in the elastic range. Our definition of the S-wave amplitude, Eq. (2), differs from that of E791. The latter includes a Gaussian form factor, so one should compare the S-wave magnitude from our analysis to the product of the E791 Gaussian form factors and magnitude. We also find a qualitative agreement between the S-wave magnitude measured by the two experiments.

FOCUS has performed a comprehensive study of the $D^+ \rightarrow K^-\pi^+\pi^+$ Dalitz plot. Using the same events, fits with the isobar model, the K-matrix formalism and the MIPWA were performed. The three fits have equivalent goodness-of-fit. The decay fractions from all fits are in good agreement. In the isobar model there is a strong correlation between the nonresonant and $\kappa\pi$ modes. Although a good fit with this model is achieved, it is difficult to disentangle the contribution of these two modes.

In Fig. 8 the S-wave phase from the three fits are compared. All fits show a good agreement in the interval $1 < m_{K\pi} < 1.35$ GeV/c^2 . The MIPWA phase is lower than those from the isobar/K-matrix fits for $m_{K\pi} < 1$ GeV/c^2 . In the high mass region the rapid variation of the phase is more pronounced in the isobar/K-matrix fits than in the MIPWA.

The S-wave magnitude from the three fits are compared in Fig. 9. In the isobar and K-matrix fits there is a broad maximum at around 0.9 GeV/c^2 , which is absent in the MIPWA fit. In the region $1.2 < m_{K\pi} < 1.4$ GeV/c^2 the MIPWA magnitude has a bump whereas in the isobar and K-matrix the magnitude decreases. In the high mass region, after the minimum, the magnitude from the MIPWA fit has a steeper variation than that of the isobar and K-matrix.

The $D^+ \rightarrow K^-\pi^+\pi^+$ decay offers an opportunity to access the $K^-\pi^+$ S-wave amplitude near threshold. Except for heavy flavor decays, no new data on the $K^-\pi^+$ system are foreseen. The ultimate goal is to extract the $I = 1/2$ $K^-\pi^+$ elastic amplitude, where all resonances are contained. The result of the MIPWA fit, however, may include other effects, such as a possible contribution of the $I = 3/2$ amplitude, or an energy dependent phase introduced by three-body final state interactions. The road from the MIPWA S-wave to the $I = 1/2$ $K^-\pi^+$ elastic amplitude is, unfortunately,

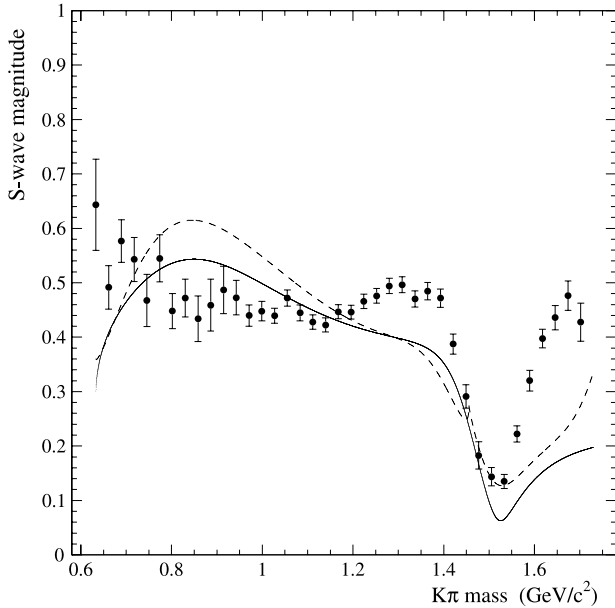


Fig. 9. Comparison between the S-wave magnitude from the three different FOCUS fits of the $K^-\pi^+\pi^+$ Dalitz plot. Points with error bars are the result of the MIPWA fit. The solid line is the central value of the isobar fit. The dashed line is the result of the K-matrix fit.

not direct. Input from theory is necessary. At this level of statistics we are already limited by systematics, which are dominated by the uncertainties on resonance parameters.

Acknowledgements

We wish to acknowledge the assistance of the staffs of Fermi National Accelerator Laboratory, the INFN of Italy, and the physics departments of the collaborating institutions. This research was supported in part by the US National Science Foundation, the US Department of Energy, the Italian Istituto Nazionale di Fisica Nucleare and Ministero della Istruzione Università e Ricerca, the Brazilian Conselho Nacional de Desenvolvimento Científico e Tecnológico and FAPERJ, CONACyT-México, and the Korea Research Foundation of the Korean Ministry of Education.

References

- [1] E.M. Aitala, et al., E791 Collaboration, Phys. Rev. Lett. 89 (2002) 121801.
- [2] M. Ablikim, et al., BES Collaboration, Phys. Lett. B 598 (2004) 149.
- [3] J.M. Link, et al., FOCUS Collaboration, Phys. Lett. B 653 (2007) 1.
- [4] G. Bonvicini, et al., CLEO-c Collaboration, Phys. Rev. D 78 (2008) 052001.
- [5] S. Descotes-Genon, B. Moussallam, Eur. Phys. J. C 48 (2006) 553.
- [6] B. Aubert, et al., BaBar Collaboration, Phys. Rev. D 76 (2007) 011102.
- [7] D. Epifanov, et al., Belle Collaboration, arXiv:0706.2231.
- [8] D. Aston, et al., LASS Collaboration, Nucl. Phys. B 296 (1988) 493.
- [9] C. Amsler, et al., Particle Data Group, Phys. Lett. B 667 (2008) 1.
- [10] J.M. Link, et al., FOCUS Collaboration, Phys. Lett. B 648 (2007) 156.
- [11] J.M. Link, et al., FOCUS Collaboration, Phys. Lett. B 585 (2004) 200.
- [12] E.M. Aitala, et al., E791 Collaboration, Phys. Rev. D 73 (2006) 032004.
- [13] P.L. Frabetti, et al., E687 Collaboration, Nucl. Instrum. Methods A 329 (1993) 62.
- [14] J.M. Link, et al., FOCUS Collaboration, Nucl. Instrum. Methods A 516 (2004) 364.
- [15] P.L. Frabetti, et al., E687 Collaboration, Nucl. Instrum. Methods A 320 (1992) 519.
- [16] J.M. Link, et al., FOCUS Collaboration, Nucl. Instrum. Methods A 484 (2002) 270.
- [17] J.M. Blatt, V.F. Weisskopf, Theoretical Nuclear Physics, John Wiley & Sons, New York, 1952.